Supplementary material for the following publication:

Surfactant-exfoliated 2D molybdenum disulphide (2D-MoS_2): the role of surfactant upon the Hydrogen Evolution Reaction

Gabriella B. de-Mello,[1,2] Lily Smith,[2] Samuel J. Rowley-Neale,[2,3] Jonas Gruber, [1] Simon J. Hutton,[4] and Craig E. Banks[2,3]*

[1]: *Escola politénica da universidade de São Paulo, Avenida, 380, CEP 05508-900, São Paulo, Brazil*

[2]: *Faculty of Science and Engineering, Manchester Metropolitan University, Chester Street, Manchester M1 5GD, UK.*

[3]: *Manchester Fuel Cell Innovation Centre, Manchester Metropolitan University, Chester Street, Manchester M1 5GD, UK.*

[4]: *Kratos Analytical Limited, Wharfside, Trafford Wharf Road, Manchester, M17 1GP*

*To whom correspondence should be addressed.

Email: c.banks@mmu.ac.uk; Tel: ++(0)1612471196; Fax: ++(0)1612476831

Website: www.craigbanksresearch.com

Liquid Exfoliation/Synthesis of 2D-MoS_2-SC

The 2D-MoS_2-SC utilised throughout this work was synthesised via a surfactant based liquid exfoliation, ultrasonication and centrifugation methodology. Liquid exfoliation was performed by placing bulk *ca.* 90 nm flake size MoS_2 powder (Sigma-Aldrich: see Experimental Section) into an aqueous solution of sodium cholate hydrate (SC: concentration, 6 g/L) within a 100 mL beaker, the resulting dispersion of bulk MoS_2 comprised a concentration of 30 g L^{-1}. This dispersion was then sonicated in a ultrasonic bath (Ultrawave, UK; 60 Hz) for 1 hour after and then centrifuged at 5000 rpm for 90 minutes. Following centrifugation, the corresponding supernatant was discarded and the resulting sediment was re-agitated/dispersed into aqueous SC (2 g L^{-1}, 100 mL). Next, the re-agitated sediment underwent further ultrasonication for a further 5 hours. Upon completion of the sonication, the solution was separated into 20 mL aliquots before each sample was centrifuged at 2000 rpm for 90 mins (separately). The sediment from this process contained un-exfoliated MoS_2 and was consequently discarded, with the remaining supernatant being subjected to a further centrifugation period at 5000 rpm for 90 minutes. Finally, the supernatant was removed containing the 2D-MoS_2-SC nanosheets that are utilised herein.

Screen-Printed Electrode Fabrication

The electrochemical measurements were performed using an Ivium Compactstat™ (Netherlands) potentiostat. Measurements were carried out using a typical three electrode system with a Pt wire counter electrode and a saturated calomel electrode (SCE) reference. The working electrodes were screen-printed graphite electrodes (SPE), which have a 3.1 mm diameter working electrode. The SPEs were fabricated in-house with the appropriate stencils using a DEK 248 screen-printing machine (DEK, Weymouth, U.K.).[1] These electrodes have been used extensively in previous studies.[2-6] In their fabrication; first a carbon-graphite ink formulation (product code C2000802P2; Gwent Electronic Materials Ltd., U.K.) was screen-printed onto a polyester (Autostat, 250 μm thickness) flexible film This layer was cured in a fan oven at 60 °C for 30 minutes. Next, a silver/silver chloride reference electrode was included by screen-printing a Ag/AgCl paste (product code C2030812P3; Gwent Electronic Materials Ltd., U.K.) onto the polyester substrates and a second curing step was undertaken where the electrodes were cured at 60 °C for 30 minutes. Finally, a dielectric paste (product code D2070423D5; Gwent Electronic Materials Ltd., U.K.) was then screen-printed onto the polyester substrate to cover the connections. After a final curing at 60 °C for 30 minutes the SPEs are ready to be used and were connected *via* an edge connector to ensure a secure electrical connection.[7]

The unmodified / bare SPEs have been reported previously and shown to exhibit a heterogeneous electron transfer rate constant, k^o, of *ca.* 10^{-3} cm s^{-1}, as measured using the $[Ru(NH_3)_6]^{3+/2+}$ outer-sphere redox probe.[8] The SPEs were modified using the drop-casting technique, where a pipette is used to manually dispense a aliquot of fluid containing the desired electrocatalyst onto an electrode's surface. This deposition is allowed to dry (at 35 ^oC) to ensure complete ethanol evaporation leaving the electrocatalyst immobilised upon the electrode surface. Finally, the electrode was allowed to cool to ambient temperature, after which the process was repeated until the desired mass was deposited onto the surface. Afterwards the modified SPE was ready to be used. This approach allows for the conventional electrochemical wiring of the electrocatalyst. The resultant product comprised surfactant (sodium cholate) exfoliated 2D-MoS_2 nanosheets (1.22 mg L^{-1}) sodium cholate (2 g L^{-1}) in an aqueous solution. Note that where surfactant control experiments were utilised, a 2 g L^{-1} solution of sodium cholate was prepared and utilised in the absence of 2D-MoS_2 (*i.e.* 2D material not present).

Characterisation Instrumentation

Transmission electron microscopy (TEM) images were obtained using JEOL 3000F high resolution transmission electron microscope (HR-TEM) with an accelerating voltage of 300 kV. The x-ray photoelectron spectroscopy (XPS) data was acquired using a AXIS Supra with a Al X-ray source (1486.6 eV) operating at 300 W for survey scans and 450 W for narrow scans. Al X-rays were monochromated using a 500 mm Rowland circle quartz crystal X-ray mirror. The angle between between X-ray source and analyser was 54.7°. With a electron energy analyser: 165 mm mean radius hemispherical sector analyser operating in fixed analyser transmission mode, pass energy 160 eV for survey scans and 40 eV narrow scans. A detector with a delay line detector with multichannel plate was utilised. X-ray diffraction (XRD) was performed using an "X'pert powder PANalytical" model with a copper source of K_α radiation (of 1.54 Å) and K_β radiation (of 1.39 Å), using a thin sheet of nickel with an absorption edge of 1.49 Å to absorb K_β radiation. The range was set between 10 and 100 2θ in correspondence with literature ranges. [9] Additionally, to ensure well defined peaks an exposure of 50 seconds per 2θ step was implemented with a size of 0.013°. Raman Spectroscopy was performed using a 'Renishaw InVia' spectrometer equipped with a confocal microscope (×50 objective) and an argon laser (514.3 nm excitation). Measurements were performed at a very low laser power level (0.8 mW) to avoid any heating effects.

Physicochemical Characterisation of the 2D-MoS_2 and 2D-MoS_2-SC

TEM was performed on the 2D-MoS_2 and 2D-MoS_2-SC nanosheets with the obtained images reported in Figure 1. The 2D-MoS_2 and 2D-MoS_2-SC have lateral widths of *ca.* 60 and 100 nm respectively with an inter nanosheet spacing of 0.33 nm. This corresponds strongly with the average values determined *via* analysis of the extinction spectra (Figure S1(D)). XRD analysis exhibit characteristic (002) diffraction peaks for the 2D-MoS_2 and 2D-MoS_2-SC nanosheets with 2θ corresponding to 14.2^0 indicating the presence of MoS_2 *via* the reflection of separated MoS_2 layers, see Figure. S1(A) which is in agreement with literature reports.[10, 11] The broad hump at 28 2θ is attributed to the supporting glass slide. Next, Raman analysis was undertaken (Figure S1(B) where the $E^1{}_2g$ and A_1g vibrational bands vibrational peaks are clearly visible at 376.8 and 402.5 cm^{-1} for the 2D-MoS_2 and 383.3 and 409.4 cm^{-1} for the 2D-MoS_2-SC. It is possible to determine the stacking number by comparison of E^1_{2g} and A_{1g} vibrational bands (VB) as the observed Raman spectrum evolves with the number of layers present. The E^1_{2g} VB results due to the opposite vibration of two S atoms in respect to a Mo atom, whereas the A_{1g} peak represents the S atoms vibrating in opposite directions and out of plane.[12, 13] As MoS_2 moves from single layer to bulk the E^1_{2g} VB downshifts from 384 to 382 cm^{-2}, whilst A_{1g} VB shifts upwards from 403 to 408 cm^{-1}, where a separation of *ca*. 19 cm^{-1} between the VBs is indicative of single layer MoS_2 and a value of *ca*. 25 cm^{-1} represents the bulk material.[13 14, 15] In both cases giving a peak ($E^1{}_2g$ - A_1g) distance of 25.7 cm^{-1}. This ($E^1{}_2g$ - A_1g) distance corresponds to the literature value expected for bulk MoS_2 (< 6 MoS_2 nanosheet layers).[6, 12, 13] Last, XPS analysis was performed to determine the elemental composition of the 2D-MoS_2 and 2D-MoS_2-SC utilised herein with Figure S1(C) showing high resolution XPS spectra for the Mo 3d and S 2d regions. The Mo and S were present at the expected ratios (1.0 : 2.2 and 1.0 : 1:7 for the 2D-MoS_2 and 2D-MoS_2-SC respectively). The XPS analysis also showed that C and O present are a result of residuals from the sodium cholate surfactant used in the fabrication of the 2D-MoS_2. The presence of a C-O component in the C 1s spectrum confirmed this, with the Na attributed to the sodium of the cholate structure. Overall, the 2D-MoS_2 and 2D-MoS_2-SC utilised in this work has been fully characterised and revealed to comprise of high quality MoS_2 nanosheets for implementation as an electrocatalyst towards the HER.

Lateral Width and Number of Layers of MoS_2 Utilised Determined *via* Optical Extinction Spectroscopy

The extinction coefficient of dispersed 2D-MoS_2 nanosheets is 6,820 L g^{-1} m^{-1} at the local minimum of 345 nm, using this information along with a spectra it is possible to determine the concentration of dispersed 2D-MoS_2 nanosheets. [16] Varrla, *et al.* [17] use this information to calculate the concentration as a function of mixing parameters whilst also showing that the extinction spectra can be used to determine information regarding the 2D-MoS_2 nanosheet length and thickness. Figure S1(D) shows the optical extinction spectra of the 2D-MoS_2 and the 2D-MoS_2-SC. It is readily evident that the spectra displays A- and B- excitonic transitions as well as other pertinent features consistent with the 2H polytype of MoS_2.[16-18] The extinction spectrum of the nanosheets allows one to readily determine the mean nanosheet lateral length due to the effect 2D-MoS_2 nanosheet edges upon the spectral profile. The extinction spectrum also allows the number of layers (thickness) to be determined as a result of quantum confinement effects causing a well-defined shift A-exciton position corresponding to nanosheet thickness .[16] The lateral length, $L(\mu m)$ of the MoS_2 can be deduced from the following equation:

$$L(\mu m) = \frac{3.5\left(Ext_B / Ext_{345}\right) - 0.14}{11.5 - \left(Ext_B / Ext_{345}\right)} \quad [1]$$

where $\left(Ext_B / Ext_{345}\right)$ is the ratio of extinction at the B-excition to that at 345 nm since the spectral profile is dependent upon the lateral length of the MoS_2. Further information can be obtained in terms of the number of nanosheets, N_{MoS_2} expressed as the number of monolayers per nanosheet can be determined from the wavelength associated with the A-excition, since the quantum conferment effects result in well-defined shifts in the A-excition position with the thickness of the nanosheet; this is summarized by the following equation:

$$N_{MoS_2} = 2.3x10^{36} e^{-54888/\lambda_A} \quad [2]$$

HER Tafel analysis of the 2D-MoS_2-SPEs

In order to ascertain the HER reaction mechanism we implemented the Tafel analysis as is common within the literature.[6] Literature has suggested three possible steps in the reaction, each of which is capable of being the rate-determining step of the HER. The initial H^+ discharge step being the Volmer reaction, leading to the following equation:[19-21]

$$H_3O^+ (aq) + e^- + \text{catalyst} \rightarrow H (ads) + H_2O (l);\ \frac{2.303RT}{\propto F} \approx 120mV$$

The Volmer step can then be followed by one of two possible steps; either the Heyrovsky step:

$$H (ads) + H_3O^+ (aq) + e^- \rightarrow H_2 (g) + H_2O (l);\ \frac{2.303RT}{(1+2)F} \approx 40mV$$

or the Tafel step:

$$H (ads) + H (ads) \rightarrow H_2 (g);\ \frac{2.303RT}{2F} \approx 30mV$$

where the transfer coefficient (α) is 0.5, F is the Faraday constant, R is the universal gas constant and T is the temperature at which the electrochemical experiment was performed at. The values from the Tafel analysis (presented below each equation) are an indication of the reaction mechanism. Tafel analysis was performed on the Faradaic sections of the LSVs shown in Figure 2(A) with the resultant Tafel slopes being exhibited in Figure 2(B). The Tafel slope values obtained for the SPE, correspond to 118, 94, 141 and 224 mV dec^{-1}.

Turn over Frequency (ToF) calculation

In order to evaluate how the intrinsic catalytic activity of the 2D-MoS_2 and 2D-MoS_2-SC on a 'per active site' basis, the ToF was deduced using a modified method reported previously.[6, 22] In this calculation is is assumed that the surface of the 2D-MoS_2 nanosheets are atomically flat (altough the true modification will have a finite roughness).[22] Taking the sulfur to sulfur bond distance to be 3.15 Å which corresponds to an area of 4.296 $Å^2$/S atom [22, 23] which can be used to calculate the surface area occupied by each MoS_2:

$$4.296 \frac{Å^2}{S\ atom} \times \frac{2\ S\ atom}{1\ MoS_2} = 8.593 \frac{Å^2}{MoS_2} \quad [1]$$

Using the dervied area for a MoS_2 molecule (corresponding to the number of surface sites for a flat standard) it is possible to determine the number of MoS_2 molecules per cm^2 geometric area:

$$\frac{1\ MoS_2}{8.593\ Å^2} \times \frac{10^{16} Å^2}{0.0707\ cm^2} = 1.646 * 10^{16} \frac{MoS_2}{cm^2} \quad [2]$$

The number of electrochemically accessible surface sites can be determined from the following:

$$\frac{\#\ Surface\ Sites\ (Catalyst)}{cm^2\ geometric\ area} = \frac{\#\ Surface\ Sites\ (Flat\ Standard)}{cm^2\ geometric\ area} \times R_F \quad [3]$$

It is also essential to accurately determine the roughness factor (R_F) for SPEs modified with 1725 ng cm^{-2} of 2D-MoS_2-SC and 1725 ng cm^{-2} of 2D-MoS_2 as is common within the literature (See Roughness Factor Calculation Section). The following allows the ToF on a per-site basis to be determined:

$$TOF\ per\ site = \frac{\#\ Total\ Hydrogen\ Turn\ Overs\ /\ cm^2\ geometric\ area}{\#\ Surface\ Sites\ (Catalyst)/\ cm^2\ geometric\ area} \quad [4]$$

Taking the value of current density (mA cm^{-2}) at the potential of –1.5 V (at a 25 mVs^{-1} scan rate) and using the R_F calculated, per-site the ToF can be deduced from the following:

$$\left(j \frac{mA}{cm^2}\right)\left(\frac{1\ A}{1000 mA}\right)\left(\frac{1\ C/s}{1\ A}\right)\left(\frac{1\ mol\ e^-}{96{,}485.3\ C}\right)\left(\frac{1\ mol\ H_2}{2\ mol\ e^-}\right)\left(\frac{6.02214*10^{23}}{1\ mol\ H_2}\right) = 1.38 \times 10^{16} \frac{H_2/S}{cm^2} per \frac{mA}{cm^2} \quad [5]$$

Using equation 6 and a value derived from formula 5, it is possible to determine a value for the ToF:

$$\left(1.34 * 10^{16} \left.\frac{\frac{H_2/S}{cm^2}}{\frac{mA}{cm^2}}\right.\right)\left(10 \frac{mA}{cm^2}\right)\left(\frac{1\ cm^2}{8.477*10^{16}\ surface\ sites}\right) = 0.375 \frac{H_2/S}{surface\ sites} \quad [6]$$

At the chosen potential (– 0.75 V) the current densities were found to correspond to -2.61 and -4.29 mA cm^{-2} for the SPEs modified with 1725 ng cm^{-2} of 2D-MoS_2-SC and 1725 ng cm^{-2} of 2D-MoS_2. Using these values the ToF values deduced from the above equations were found

to correspond to 0.191 and 0.314 $\frac{H_2/S}{\text{Surface Site}}$ respectively.

Roughness Factor (R_F) Calculation

Modifying the method of Shin *et al.* [24] and Rowley *et al*.[6] the double layer capacitance can be used to calculate the electrochemically active surface area of the 2D-MoS_2-SPEs. Cyclic voltammetry was performed using a potential range of 0.01 to 0.11 V, which is within the non-Faradaic window, at each of the following scan rates (20, 40, 60, 80, 100 mVs^{-1}). The potential range used is presumed to have no Faradaic processes occurring, therefore cathodic and anodic current densities are associated with charging of the electrical double layer. Figure S2 shows the difference between the anodic and cathodic current at 0.06 V *versus* the corresponding scan rate. The slope of each set of points in Figure S2 being proportional to a doubling of the double layer capacitance. The double layer capacitance values determined are 11, 242, 288 and 294 $\mu F\ cm^{-2}$ of bare/unmodified SPE, SPE modified with *ca*. 2.8 mg cm^{-2} of SC, SPE modified with *ca*. 1725 ng cm^{-2} of 2D-MoS_2, SPE modified with *ca*. 1725 ng cm^{-2} of 2D-MoS_2-SC modified respectively. The R_F values are used in the previous ToF calculations.

Table S1. Comparison of literature reporting surfactant fabricated MoS_2 based catalysts that been explored towards the HER

Electrocatalyst	Surfactant	Supporting Electrode	Electrolyte	HER onset (–V)	Tafel Value (mV dec^{-1})	Reference
MoS_2 nanospheres	PVP	GC	0.5 M H_2SO_4	0.11 (*vs*. RHE)	72	[25]
MoS_2 nanosheets	CTAB	GC	0.5 M H_2SO_4	0.09 *(vs*. RHE)	55	[26]
MoS_2-SWNT	SDS	GC	0.5 M H_2SO_4	0.20 *(vs*. RHE)	60	[27]
MNTs@rGO	octylamine	GC	0.5 M H_2SO_4	0.18 (*vs*. RHE)	69	[28]
2D-MoS_2-SC	SC	SPEs	0.5 M H_2SO_4	0.61 *(vs.* SCE)	141	*This work*
2D-MoS_2	none	SPEs	0.5 M H_2SO_4	0.42 *(vs.* SCE)	94	*This work*

Key: PVP: poly(vinylpyrrolidone); GC:glassy carbon; RHE: relative hydrogen electrode; CTAB: cetyltrimethyl ammonium bromide; SWNT: single walled nanotubes; SDS: sodium dodecylsulfate; MNT: MoS_2 nanotubes; rGO: reduced graphene oxide: SC: sodium cholate: SPEs: screen-printed electrodes.

Figure S1. Characterisation of the 2D-MoS_2 and 2D-MoS_2-SC; (A) XRD (deposited on a glass slide), (B) Raman spectra (deposited onto a silicon wafer between 300 and 500 cm^{-1}). (C) High resolution XPS spectra for the Mo 3d and S 2d regions of 2D-MoS_2 and 2D-MoS_2-SC. (D) Extinction spectra (nanosheets dispersed in ethanol (1.22 mg L^{-1})).

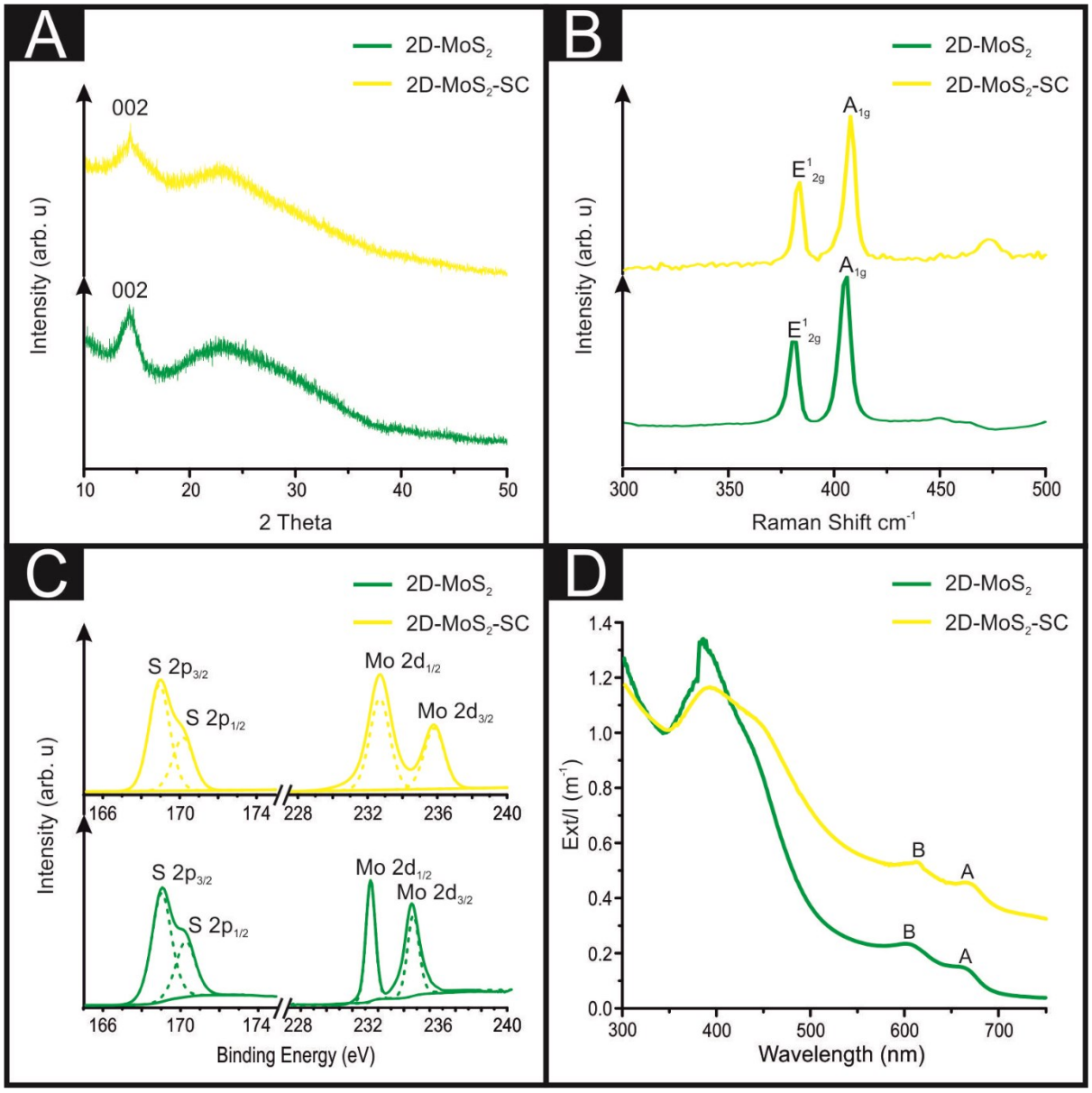

Figure S2. The difference in anodic and cathodic current density (potential range 0.01 to 0.11 V) taken at +0.06 V *versus* scan rate (mV s^{-1} *vs.* SCE) for a bare/unmodified SPE, SPE modified with *ca*. 2.8 mg cm^{-2} of SC, SPE modified with *ca*. 1725 ng cm^{-2} of 2D-MoS_2 and a SPE modified with *ca*. 1725 ng cm^{-2} of 2D-MoS_2-SC. The slope of the linear regression indicates the value of double layer capacitance (C_{dl}: µF cm^{-2}).

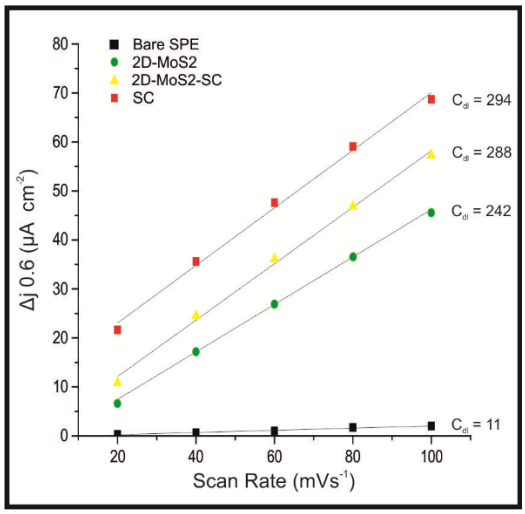

References

1. N. A. Choudry, D. K. Kampouris, R. O. Kadara and C. E. Banks, *Electrochem. Commun.*, 2010, 12, 6-9.
2. L. R. Cumba, J. P. Smith, D. A. C. Brownson, J. Iniesta, J. P. Metters, D. R. D. Carmo. and C. E. Banks, *Analyst*, 2015, 140, 1543-1550.
3. C. W. Foster, J. Pillay, J. P. Metters and C. E. Banks, *Sensors (Basel, Switzerland)*, 2014, 14, 21905-21922.
4. C. W. Foster, J. P. Metters and C. E. Banks, *Electroanalysis*, 2013, 25, 2275-2282.
5. J. P. Metters, M. Gomez-Mingot, J. Iniesta, R. O. Kadara and C. E. Banks, *Sens. Actuators, B*, 2013, 177, 1043-1052.
6. S. J. Rowley-Neale, D. A. C. Brownson, G. C. Smith, D. A. G. Sawtell, P. J. Kelly and C. E. Banks, *Nanoscale*, 2015, 7, 18152-18168.
7. F. E. Galdino, C. W. Foster, J. A. Bonacin and C. E. Banks, *Anal. Methods*, 2015, 7, 1208-1214.
8. S. J. Rowley-Neale, D. A. C. Brownson and C. E. Banks, *Nanoscale*, 2016, 8, 15241-15251.
9. Z. Lei, S. Xu and P. Wu, *Phys. Chem. Chem. Phys.*, 2016, 18, 70-74.
10. P. C. Joensen, E. D. Alberding, N. Frindt, R. F., *J. Phys. C: Solid State Phys.*, 1987, 20, 4043-4053.
11. S. S. Chou, M. De, J. Kim, S. Byun, C. Dykstra, J. Yu, J. Huang and V. P. Dravid, *J. Am. Chem. Soc.*, 2013, 135, 4584-4587.
12. H. Li, Q. Zhang, C. C. R. Yap, B. K. Tay, T. H. T. Edwin, A. Olivier and D. Baillargeat, *Adv. Funct. Mater.*, 2012, 22, 1385-1390.
13. C. Lee, H. Yan, L. E. Brus, T. F. Heinz, J. Hone and S. Ryu, *ACS Nano*, 2010, 4, 2695-2700.
14. F. Cesano, S. Bertarione, A. Piovano, G. Agostini, M. M. Rahman, E. Groppo, F. Bonino, D. Scarano, C. Lamberti, S. Bordiga, L. Montanari, L. Bonoldi, R. Millini and A. Zecchina, *Catal. Sci. Technol.*, 2011, 1, 123-136.
15. D. Y. Chung, S.-K. Park, Y.-H. Chung, S.-H. Yu, D.-H. Lim, N. Jung, H. C. Ham, H.-Y. Park, Y. Piao, S. J. Yoo and Y.-E. Sung, *Nanoscale*, 2014, 6, 2131–2136.
16. C. Backes, R. J. Smith, N. McEvoy, N. C. Berner, D. McCloskey, H. C. Nerl, A. O'Neill, P. J. King, T. Higgins, D. Hanlon, N. Scheuschner, J. Maultzsch, L. Houben, G. S. Duesberg, J. F. Donegan, V. Nicolosi and J. N. Coleman, *Nat Commun*, 2014, 5.
17. E. Varrla, C. Backes, K. R. Paton, A. Harvey, Z. Gholamvand, J. McCauley and J. N. Coleman, *Chem. Mater.*, 2015, 27, 1129-1139.
18. J. A. Wilson and A. D. Yoffe, *A. D. Adv. Phys.*, 1969, 19, 193-335.
19. N. M. Marković, B. N. Grgur and P. N. Ross, *J. Phys. Chem. B*, 1997, 101, 5405-5413.
20. N. M. Marković and P. N. R. Jr, *Surf. Sci. Rep.*, 2002, 45, 117-229.
21. A. B. Laursen, S. Kegnaes, S. Dahl and I. B. Chorkendorff, *Energy Environ. Sci.*, 2012, 5, 5577-5591.
22. J. D. Benck, Z. Chen, L. Y. Kuritzky, A. J. Forman and T. F. Jaramillo, *ACS Catal.*, 2012, 2, 1916-1923.
23. S. Helveg, J. V. Lauritsen, E. Lægsgaard, L. Stensgaard, J. K. Nørskov, B. S. Clausen, H. Topsøe and F. Besenbacher, *Phys. Rev. Lett.*, 2000, 84, 951-954.
24. S. Shin, Z. Jin, D. H. Kwon, R. Bose and Y.-S. Min, *Langmuir*, 2015, 31, 1196-1202.
25. S. Zhang, B. V. R. Chowdari, Z. Wen, J. Jin and J. Yang, *ACS Nano*, 2015, 9, 12464-12472.
26. Z. Guo, Q. Ma, Z. Xuan, F. Du and Y. Zhong, *RSC Adv.*, 2016, 6, 16730-16735.
27. D. Voiry, M. Salehi, R. Silva, T. Fujita, M. Chen, T. Asefa, V. B. Shenoy, G. Eda and

M. Chhowalla, *Nano Lett.*, 2013, 13, 6222-6227.
28. L. Song, M. Zhao, X. Li, Z. Zhang and L. Qu, *RSC Adv.*, 2016, 6, 70740-70746.